Investigation of Pr2NiMnO6-Ce0.9Gd0.1O1.95 composite cathode for intermediate-temperature solid oxide fuel cells

Huan Li, Li-Ping Sun, Qingmao Feng, Li-Hua Huo, Hui Zhao, Jean-Marc. Bassat, Aline Rougier, Sébastien Fourcade, Jean-Claude Grenier

ORIGINAL PAPER

Investigation of Pr_2NiMnO_6-$Ce_{0.9}Gd_{0.1}O_{1.95}$ composite cathode for intermediate-temperature solid oxide fuel cells

Huan Li[1] · Li-Ping Sun[1] · Qingmao Feng[1] · Li-Hua Huo[1] · Hui Zhao[1] · Jean-Marc Bassat[2] · Aline Rougier[2] · Sébastien Fourcade[2] · Jean-Claude Grenier[2]

Abstract The electrochemical performance of Pr_2NiMnO_6 (PNMO)-$x Ce_{0.9}Gd_{0.1}O_{1.95}$ (CGO) (x = 0–40 wt%) composite oxides as intermediate-temperature solid oxide fuel cell (IT-SOFC) cathode materials are evaluated. The electrochemical impedance spectroscopy (EIS) analysis results identify two consecutive electrode processes on the composite cathode. Among the various composites, PNMO-30CGO cathode exhibits the best electrochemical performance with the minimum polarization resistance of 0.23 Ω cm^2 and the maximum exchange current density of 75 mA cm^{-2} at 700 °C in air. These values are almost constant even after 30-h operation. The oxygen reduction reaction (ORR) mechanism studies prove that the major rate-determining step is the charge-transfer process. Introducing CGO significantly improves the charge-transfer process, by increasing the triple phase boundary (TPB) length and oxygen vacancy concentration in the composite cathode.

Keywords Solid oxide fuel cells · Double perovskite · Composite cathode · Oxygen reduction reaction mechanism

✉ Li-Ping Sun
lipingsun98@yahoo.com

✉ Hui Zhao
zhaohui98@yahoo.com

[1] Key Laboratory of Functional Inorganic Material Chemistry, Ministry of Education, School of Chemistry and Materials Science, Heilongjiang University, Harbin 150080, People's Republic of China

[2] CNRS, Université de Bordeaux, ICMCB, 87 Avenue du Dr. A. Schweitzer, F-33608 Pessac-Cedex, France

Introduction

Solid oxide fuel cells (SOFCs), as an energy conversion device with high efficiency and low pollution emission, have attracted much attention over the last decades. To accelerate the widespread application of SOFCs, a recognized research direction is to reduce the operation temperature from high temperature (HT, 800–1000 °C) to intermediate temperature (IT, 500–700 °C) [1–3]. With the reduction of operation temperature, a series of problems emerge related to large cathodic polarization loss and poor catalytic activity for oxygen reduction reaction (ORR) [4]. It is necessary to improve the cathode electrochemical performance and reveal the ORR mechanism.

To date, the mixed ionic-electronic conductors (MIECs) with the desirable physicochemical characteristics present superior electrochemical performance in IT-SOFCs. It is generally accepted that the ORR occurred on porous MIEC cathodes involves five overlapping processes: (1) gas oxygen diffusion to the cathode, (2) molecular oxygen surface adsorption on cathode, (3) surface diffusion and dissociation of molecular oxygen, (4) charge-transfer process, and (5) the transport process for oxygen ions from the cathode into the electrolyte [5–10]. In order to improve the ORR properties and the electrochemical performance, much efforts have been paid to ameliorate these five overlapping processes. An effective and common method is introducing ionic conduction phase, such as $Ce_{1.9}Gd_{0.1}O_{1.95}$ (CGO), to form composite cathode. This approach increases the triple phase boundary (TPB) length, promotes oxygen transport process, and leads to the improvement of ORR [11–14]. For example, the addition of CGO in $La_{0.6}Sr_{0.4}Co_{0.2}Fe_{0.8}O_3$ (LSCF) results in significant decrease of the polarization resistance [12]. The similar improvement was also observed in $La_{0.8}Sr_{0.2}MnO_3$ (LSM)-CGO composite cathode [15]. Other papers reported the conspicuous effects on the thermal expansion coefficients (TECs) and compatibility

of the composite cathode with electrolyte [16]. Therefore, incorporation of CGO into the electrode material is a good option to improve the electrochemical performance of the cathode. In our previous study, Pr_2NiMnO_6 (PNMO) was investigated as cobalt-free cathode material for IT-SOFCs, which exhibited comparable TECs and high-temperature chemical compatibility with CGO electrolyte [17]. However, the polarization resistance of PNMO cathode is still larger than the well-known cathode [18]. In this paper, we present a systematic investigation of the PNMO-*x*CGO composite cathode. The effect of CGO contents on the ORR mechanism is further investigated.

Experimental

Sample preparation

PNMO powder was prepared by glycine nitrate process (GNP). Briefly speaking, analytical grade Pr $(NO_3)_3{\cdot}6H_2O$, Ni $(NO_3)_2{\cdot}6H_2O$, and Mn $(NO_3)_2{\cdot}4H_2O$ were used as raw materials and dissolved in a stoichiometric ratio in distilled water. Glycine was then added to the solution with a molar ratio of 3 glycine to 1 metal ion as chemical propellant. After drying and firing, the precursor was calcined in air at 950 °C for 10 h to form PNMO powder.

The CGO electrolyte substrate (with density ~93 %) was prepared according to our previous publication [17]. The cathode inks were prepared by mixing certain amounts of CGO powder with PNMO in ethyl cellulose-terpineol binder and denoted as PNMO-*x*CGO (*x* = 0–40 wt%). Two kinds of test cells were prepared, and their configurations were schematically presented in Fig. 1. For the symmetrical cell, the cathode ink was printed on both sides of CGO electrolyte in square shape area of 0.25 cm^2 at the symmetrical position and sintered at 1000 °C for 4 h in air. The platinum paste was printed on electrode surface to act as current collector. The cathode thickness and loading density were approximately 20 μm and 6.5 g cm^{-3}, respectively. For three-electrode cell, the cathode ink was painted on one side of the CGO electrolyte to form the working electrode (*WE*) with an area of 0.25 cm^2, followed by firing at 1000 °C for 4 h in air. Platinum paste was printed to the opposite side as the counter electrode (*CE*). A Pt wire was used as reference electrode (*RE*) and put on the same side of *WE*, followed by firing at 800 °C for 1 h in air.

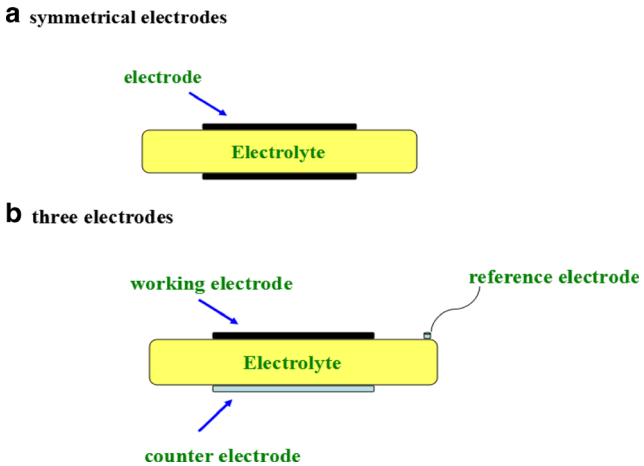

Fig. 1 The schematic illustration for electrode configuration: **a** symmetrical electrodes and **b** three electrodes

Characterizations

The crystal structure, phase purity, and chemical compatibility of cathode materials were confirmed by the X-ray diffraction (XRD) measurement. The condition of the data collection was in the 2θ range of 20°–80° with increments of 0.02° by using Cu-Kα radiation. The microstructure of the electrode was

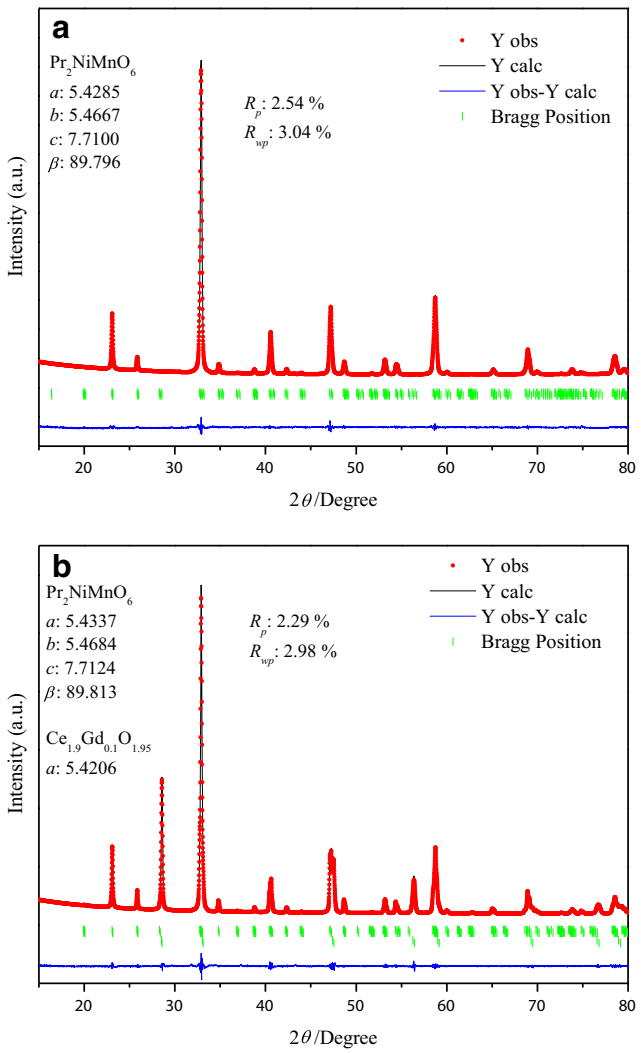

Fig. 2 **a** X-ray diffraction (XRD) pattern refinement results of Pr_2NiMnO_6 powders synthesized by GNP method and **b** XRD patterns of Pr_2NiMnO_6-30CGO mixture after sintered at 1000 °C for 12 h in air

investigated by field emission scanning electron microscope (FESEM, Hitachi, S-4700 FEG). The electrochemical performance was characterized by electrochemical workstation (AUTOLAB, PGSTAT30) under open-cell voltage (OCV). The applied frequency ranged from 1 MHz to 0.01 Hz, and the signal amplitude is 50 mV. The measurements were performed as a function of temperature (500–700 °C) and oxygen partial pressure controlled by N_2 (99.99 %)/O_2 (99.99 %) mixed atmosphere. The dc polarization experiments are performed according to the procedure in literature [19].

Results and discussion

Figure 2a shows the XRD pattern refinement results of PNMO powders synthesized by GNP method. The material crystallizes in single phase with monoclinic double perovskite structure (space group $P2_1/n$) [20]. The refinement results converged excellently with discrepancy factors R_p = 2.54 % and R_{wp} = 3.04 %. The unit cell parameters a = 5.428(5) Å, b = 5.466(7) Å, c = 7.710(0) Å, and β = 89.79(6)° are in good agreement with the previous studies [20], which indicates that pure phase PNMO is successfully prepared by GNP method. Compared to the cell parameters of PNMO prepared by solid-state reaction [17], the material prepared by GNP method shows much expanded cell parameters and inclined β value. This difference may come from the different synthesis methods. Pure phase PNMO can be obtained by GNP method at 950 °C for 10 h, whereas for solid-state reaction, it is 1400 °C for 24 h. To examine the chemical compatibility between PNMO and CGO, the two powders were mixed in a weight ratio of 1:1 and heated at 1000 °C for 10 h in air. The XRD pattern refinement results of the heat-treated mixture are shown in Fig. 2b. The obtained cell parameters of PNMO are

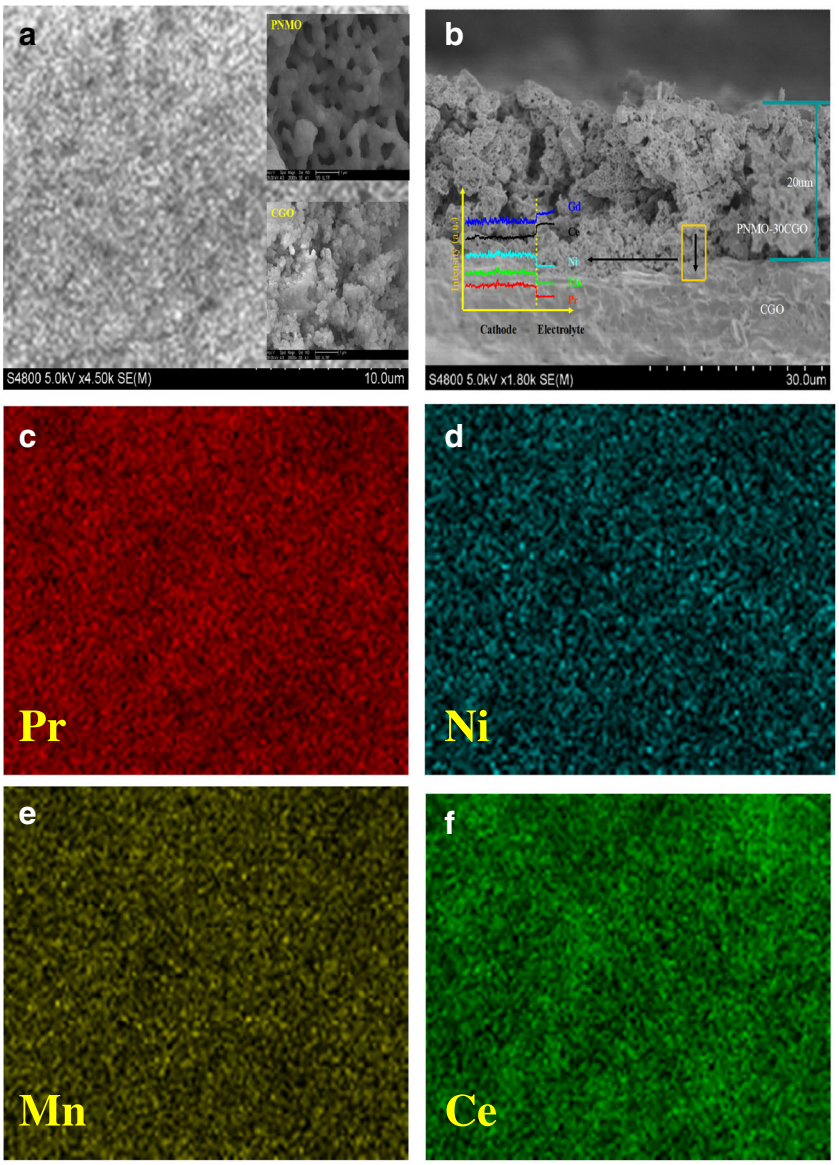

Fig. 3 **a**, **b** SEM micrographs of Pr_2NiMnO_6-30CGO composite cathode on CGO electrolyte after sintered at 1000 °C for 4 h. **c–f** Mapping results of elements. *Inset* of **a** shows SEM images of PNMO and CGO. *Inset* of **b** shows the elemental profiles obtained from the EDX line scan

a = 5.433(7) Å, b = 5.468(4) Å, c = 7.712(4) Å, and β = 89.81(3)°, quite similar to the result of Fig. 2a. CGO crystallizes in cubic fluorite-type structure, and the cell parameters are $a = b = c = 5.420(6)$ Å, which is in good agreement with the data of JCPDS card no. 01-075-0161. These results reveal that PNMO and CGO remain in their own structures; no obvious interface reaction or solid solution formation is found. It concludes that PNMO is a chemically stable cathode material on CGO electrolyte.

The microstructure of the electrode is very important for achieving excellent electrochemical performance, because it is related to the process of electron and charge transfer. An optimum cathode microstructure should have large TPB, suitable particle size, and high porosity. The SEM images of the surface and cross section of the PNMO-30CGO composite cathode are shown in Fig. 3a–b. It is found that the average particle size of PNMO and CGO is approximately 0.32 and 0.17 μm (inset of Fig. 3a), respectively. The cross-section image shows that the thickness of the cathode layer is approximately 20 μm (Fig. 3b). Figure 3c–f present the energy dispersive X-ray spectroscopy (EDX) mapping results of Pr, Ni, Mn, and Ce elements obtained from the porous PNMO-30CGO cathode surface. Clearly, the composition elements distribute uniformly in the cathode. In order to identify the high-temperature chemical stability of PNMO-30CGO, the EDX line scan was performed across the interface of CGO electrolyte and PNMO cathode. The scan results are superimposed in Fig. 3b. The elemental profiles obtained from the EDX analysis correspond well with the chemical compositions of different layers and ensure the absence of interfacial reactions between electrolyte and cathode materials. This result is in agreement with that obtained from the XRD refinement results in Fig. 2b.

The electrochemical performance of PNMO-xCGO composite cathodes with different CGO content was evaluated by electrochemical impedance spectroscopy (EIS). The measurements were conducted on the symmetric cells at 700 °C under OCV. The typical EIS spectra were shown in Fig. 4a. The difference between the high-frequency (HF) and low-frequency (LF) intercept values on real axis is attributed to the total polarization resistance (R_p). It is observed that CGO content makes significant effects on polarization resistance. R_p decreases first with the increase of CGO content. The lowest R_p value of 0.23 Ω cm^2 is obtained with 30 wt% CGO, which is about two times smaller than that of the pure PNMO cathode. The optimum composition of PNMO-xCGO composite cathodes can be understood by the effective medium percolation theory (EMPT) [12, 21]. It implies that the superior electrochemical performance of the composite cathode is associated with the component particle size. For example, Chen et al. found that the optimum YSZ volume fraction (YSZ) with minimum R_p in LSM-YSZ composite cathode was related to the ratio of particle size (rYSZ/rLSM), varying from YSZ = 0.24 for rYSZ/rLSM = 0.2 to YSZ = 0.55 for

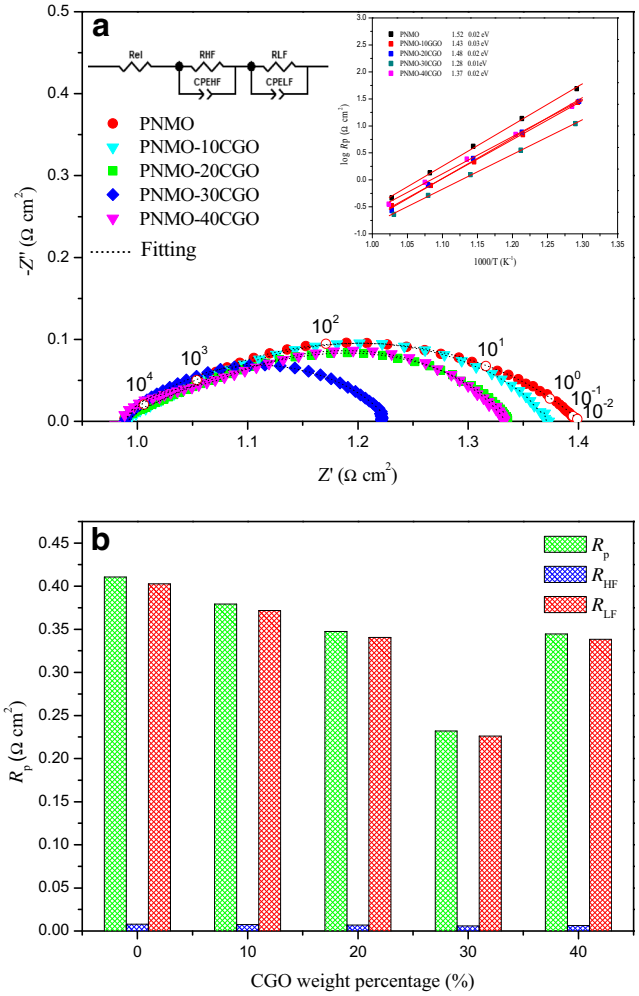

Fig. 4 **a** Impedance spectra of the composite cathodes at 700 °C under open circuit potential. *Inset* shows the arrhenius plot of R_p values for Pr_2NiMnO_6-xCGO (x = 0–40 wt%) composite cathodes. **b** The histogram of R_{HF}, R_{LF}, and R_p with CGO contents

rYSZ/rLSM = 1 [22]. Considering that the grain size of PNMO is larger than that of CGO and the ratio of rCGO/rPNMO is about 0.53, the optimum CGO weight fraction in PNMO-xCGO composite cathodes is therefore approximately 30 wt% (~35 vol%). By surveying the literature, there are many papers dealing with ceria-containing composites for IT-SOFCs. The physicochemical and electrochemical properties of several known cathodes and their corresponding composite cathodes are comparably presented in Table 1. From the table, we can see that both the composition and structure have great influence to the R_p values. Normally, the cobalt composite materials have the best ORR properties. For the cobalt-free materials, it is found that PNMO-xCGO exhibits comparable TECs and relatively low polarization resistance, which indicates that it can be regarded as a promising cobalt-free cathode material. A noteworthy result in Table 1 should be mentioned for LSCF-CGO composite cathode. Clearly, the composite cathode prepared by infiltration and electrospinning methods exhibits significantly improved electrochemical performance

Table 1 Comparisons of physicochemical and electrochemical properties of some known cathodes and their corresponding composite cathodes in the literature

Materials	σ (S cm^{-1})/T (°C)	TEC (K^{-1})	R_p (Ω cm^2)/T (°C)	Reference
$La_{0.8}Sr_{0.2}MnO_3$ + CGO	99.33/1000	11.6×10^{-6}	8.20/800	[23]
	–	–	0.39/800	[24]
$La_{0.6}Sr_{0.4}Co_{0.2}Fe_{0.8}O_3$ + CGO	300/600~800	15.3×10^{-6}	1.20/600	[25, 26]
	–	–	0.27/600	[26]
			0.10/650 (Infiltration)	[27]
			0.07/650 (Electrospinning)	[28]
$LaNi_{0.6}Fe_{0.4}O_3$ + CGO	580/800	/11.4×10^{-6}	0.70/750	[29]
	–	–	0.28/700	[30]
$La_2NiO_{4+\delta}$ + CGO	70/700	13.8×10^{-6}	0.38/800	[31–33]
	–	–	0.15/600	[34]
Pr_2CuO_4 + CGO	100/900	11.8×10^{-6}	0.56/700	[35, 36]
	–	–	0.41/700	[37]
$EuBaCo_2O_{5+\delta}$ + CGO	100/423	14.9×10^{-6}	0.50/600	[38]
	78/750	12.0×10^{-6}	0.05/700	[39]
Pr_2NiMnO_6 + CGO	3.0/800	10.6×10^{-6}	0.38/700	[17]
	–	–	0.23/700	This work

CGO $Ce_{0.9}Gd_{0.1}O_{1.95}$

than the mechanical mixing method [27, 28], which provides hints for us to improve the electrochemical performance of PNMO-*x*CGO composite cathode in the future work. The Arrhenius plots of R_p with CGO contents are shown in Fig. 4a (inset). The activation energy (*E*a) of the composite cathode is in the range of 1.52(±0.02)–1.28(±0.01) eV. The lowest *E*a value is obtained in PNMO-30CGO. The calculated activation energy is somehow different to the PNMO cathode prepared by solid-state reaction [17]. The reason may come mainly from the different electrode sintering temperatures. Normally, the change of ORR mechanism will lead to great change of activation energy [26]. As the *E*a value of PNMO-*x*CGO composite cathode shows less significant change with CGO contents, this result indicates that introducing CGO does

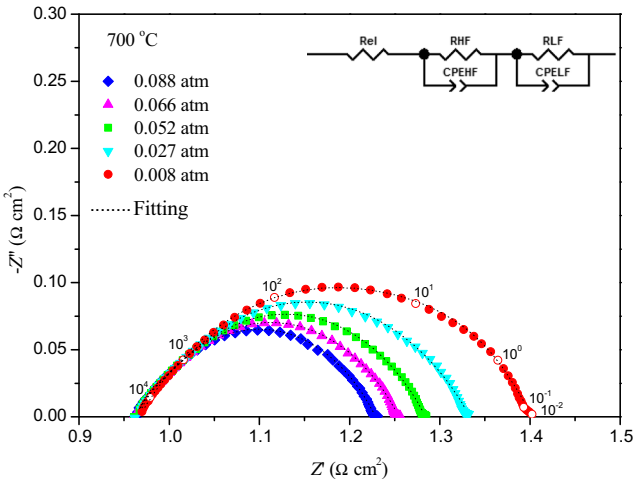

Fig. 5 Nyquist plot of Pr_2NiMnO_6-30CGO composite cathode measured at 700 °C under various oxygen partial pressures

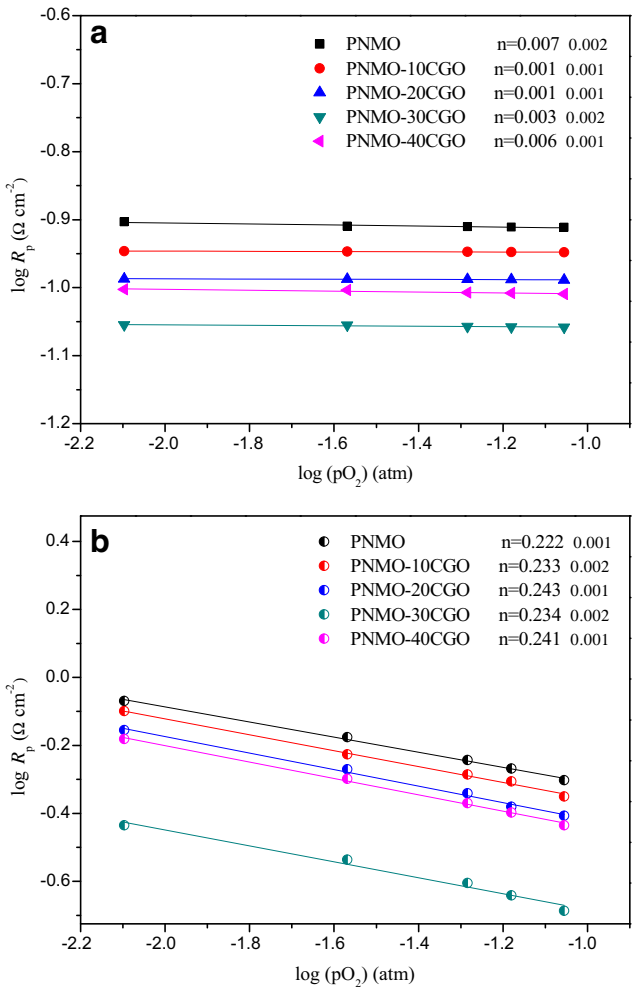

Fig. 6 The dependence of R_p on oxygen partial pressure at 700 °C

not change the ORR mechanism. The similar result has been observed in $SmBaCo_2O_{5+\delta}$-CGO composite cathode [16].

The impedance spectra of PNMO-*x*CGO cathode can be divided into two arcs in HF and LF zone, respectively. This suggests that there are at least two different processes occurred on the cathode. In order to clarify these processes, an equivalent circuit with the model of R_{el}-(R_{HF}//CPE_{HF})-(R_{LF}//CPE_{LF}) is used to separate the two arcs in the whole frequency zone. In this equivalent circuit, R_{el} is described as the overall resistance related to the ohmic contribution of the electrolyte, the current collector, electrode, and leads. *R* and CPE in parallel (*R*//CPE series) is attributed to the polarization resistance and constant phase element, respectively. The fitting results of high-frequency arc (R_{HF}), low-frequency arc (R_{LF}), and R_p (total polarization resistance, $R_p = R_{HF} + R_{LF}$) are shown in Fig. 4b. It is found that R_{LF} is much larger than R_{HF}, indicating the low-frequency reaction process as the major rate-limiting step. In addition, from the variation of R_{HF} and R_{LF} with CGO content, it can be concluded that the main contribution of reducing R_p comes from the improvement of low-frequency process.

To clarify the ORR kinetics of PNMO-30CGO composite cathode, the polarization resistance was further measured under various oxygen partial pressures (Fig. 5). The same equivalent circuit in Fig. 4a was used to identify the different electrochemical processes. The fitting results of R_{HF} and R_{LF} as a function of oxygen partial pressure are presented in Fig. 6a, b, respectively. It is observed that R_{LF} increases with the decrease of oxygen partial pressure, whereas R_{HF} remains almost unchanged. The variation of R_p with oxygen partial pressure can be described by the formula $R_p = R_p^o \times (P_{O_2})^{-n}$. The parameter *n* is used to identify the different electrochemical processes [7, 40–43], as that schematically illustrated in Fig. 7.

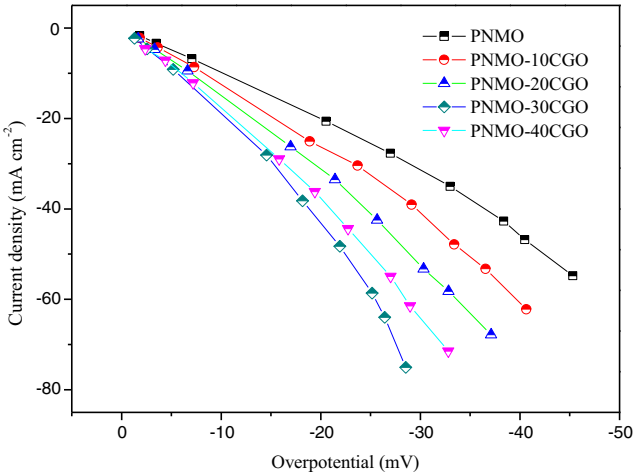

Fig. 8 The overpotential-current density curves of Pr_2NiMnO_6-*x*CGO (*x* = 0–40 wt%) measured at 700 °C in air

The values of *n* for HF arc and LF arc are around 0 and 0.25, implying that HF arc represents the diffusion of oxygen ions from TPB to electrolyte and LF arc is the charge-transfer process. It is found from Fig. 6 that R_{LF} is always larger than R_{HF}, which means that the charge-transfer process is the major determining step of ORR reaction on PNMO-*x*CGO composite cathodes. The addition of CGO seems to greatly promote the charge-transfer process (Fig. 4b). This phenomenon can be understood, considering the substantial increase of TPB length and the generation of more active sites and oxygen vacancies in the composite electrode, which is beneficial to the charge-transfer reaction. However, when the CGO content reaches to 40 wt%, the value of R_{LF} increases again. This may be due to the block of electron-conducting path within the PNMO particles by the high content CGO particles.

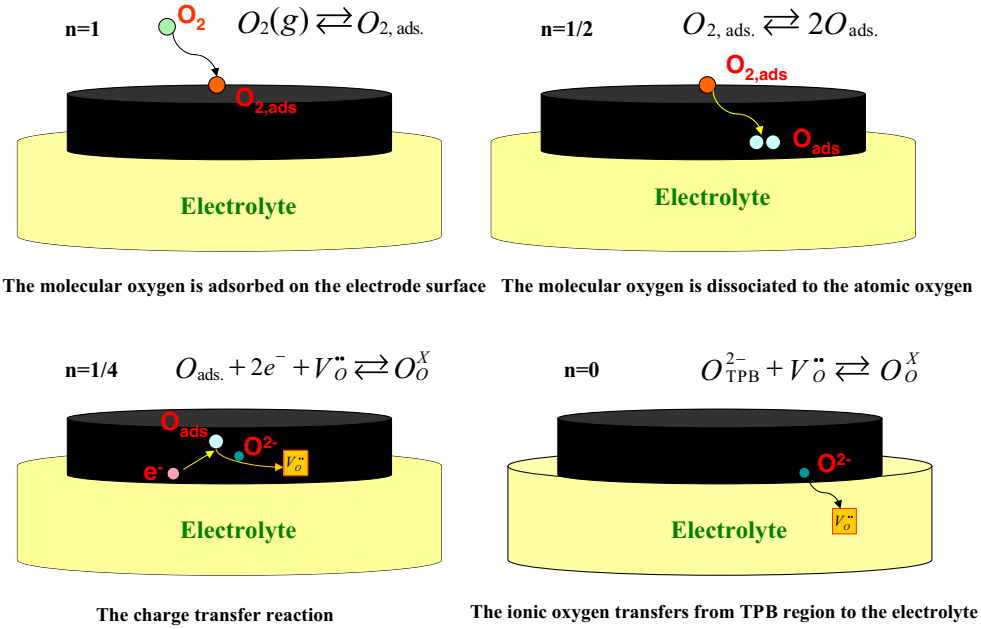

Fig. 7 The schematic illustrations of oxygen reduction reaction processes

As an important parameter, cathode overpotential is measured to evaluate the effect of CGO content on the polarization properties of PNMO-*x*CGO composite cathodes. Figure 8 shows the overpotential-current density curves measured at 700 °C in air. Under the same overpotential, the current density increases with the addition of CGO. The maximum current density of 75 mA cm^{-2} at the overpotential of 28 mV is obtained in PNMO-30CGO composite cathode. The result indicates that introducing CGO makes significant effect on the electrode performance and electrocatalytic activity of Pr_2NiMnO_6-*x*CGO composite cathode.

The electrochemical stability of PNMO-30CGO composite cathode was further characterized. The Nyquist plots measured at 700 °C for 10, 20, and 30 h are comparably shown in Fig. 9a. It is observed that R_p value does not change significantly with the operation time. In addition, the chronoamperometric plot of the composite cathode is shown in Fig. 9b. The current density remains almost constant during 30 h at 700 °C in air. These results prove that PNMO-30CGO composite cathode has good electrochemical stability.

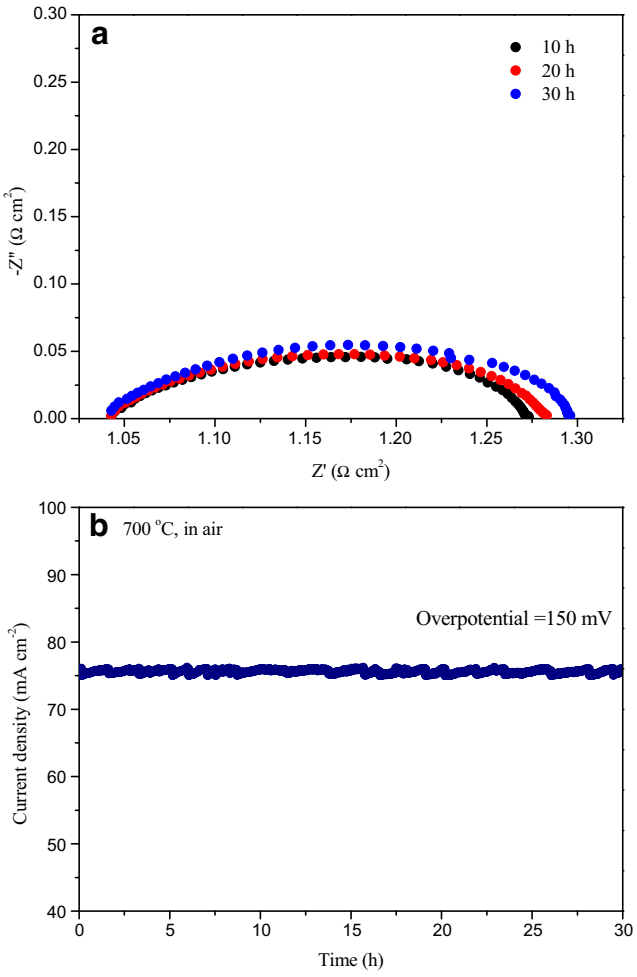

Fig. 9 **a** The Nyquist plots of Pr_2NiMnO_6-30CGO composite cathode after keeping at 700 °C for 10, 20, and 30 h. **b** The chronoamperometric curve of the composite cathode at 700 °C under overpotential 150 mV for 30 h

Conclusions

The PNMO-*x*CGO composite oxides were investigated as potential cathode materials for IT-SOFCs. The addition of CGO to PNMO made a significant effect on the electrochemical performance, owing to the increase of TPB length, oxygen vacancy concentration, and active site. The PNMO-30CGO composite cathode exhibited the lowest R_p value of 0.23 Ω cm^2 at 700 °C in air and the maximum current density of 75 mA cm^{-2} at the overpotential of 28 mV. The oxygen partial pressure dependence study indicated that the major rate-limiting step was the charge-transfer process. In addition, PNMO-30CGO composite cathode exhibited good electrochemical stability at 700 °C.

Acknowledgments The project was supported by National Natural Science Foundation of China (51302069, 51372073), Foundation of Heilongjiang Educational Department (2013TD002), Nature Science foundation of Heilongjiang Province in China (E2016051), Scientific Research Foundation for Returned Scholars, and Ministry of Human Resources and Social Security of People's Republic of China (2014-240).

References

1. Adler SB (2004) Chem Rev 104:4791–4843
2. Jacobson AJ (2010) Chem Mater 22:660–674
3. Zhou W, Liang FL, Shao ZP, Zhu ZH (2012) Sci Rep 2:327–333
4. Brett DJL, Atkinson A, Brandon NP, Skinner SJ (2008) Chem Soc Rev 37:1568–1578
5. Wang DY, Nowick AS (1979) J Electrochem Soc 126(7):1155–1165
6. Takeda Y, Kanno R, Noda M, Yamamoto O (1987) J Electrochem Soc 134:A2656–A2661
7. Sicbeit E, Hammouche A, Kleitz M (1995) Electrochim Acta 40: 1741–1753
8. Sun LP, Li Q, Zhao H, Hao JH, Huo LH, Pang GS, Shi Z, Feng SH (2012) Int J Hydrog Energy 37:11955–11962
9. Escudero MJ, Aguadero A, Alonso JA, Daza L (2007) J Electroanalyt Chem 611:107–116
10. Wang JP, Meng FC, Xia T, Shi Z, Lian J, Xu CB, Zhao H, Bassat JM, Grenier JC (2014) Int J Hydrog Energy 39:18392–18404
11. Adler SB, Lane JA, Steele BCH (1996) J Electrochem Soc 143: 3554–3564
12. Murray EP, Sever MJ, Barnett SA (2002) Solid State Ionics 148: 27–34
13. Sun LP, Rieu M, Viricelle JP, Pijolat C, Zhao H (2014) Int J Hydrog Energy 39:1014–1022
14. Shi Z, Xia T, Meng FC, Wang JP, Zhao H, Xu CB (2015) Electrochim Acta 174:608–614
15. Murray EP, Barnett SA (2001) Solid State Ionics 143:265–273
16. Lü SQ, Long GH, Ji Y, Meng XW, Sun CC (2010) Int J Hydrog Energy 35:7930–7935
17. Li H, Sun LP, Li Q, Xia T, Zhao H, Huo LH, Bassat JM, Rougier A, Fourcade S, Grenier JC (2015) Int J Hydrog Energy 40:12761–12769

18. Shao ZP, Haile SM (2004) Nature 431:170–173
19. Li Q, Xia T, Sun LP, Zhao H, Huo LH (2014) Electrochim Acta 150:151–156
20. Zhang G, Li G, Liao F, Fu Y, Xiong M, Lin J (2011) J Cryst Growth 327:262–266
21. Patro PK, Delahaye T, Bouyer E (2011) Solid State Ionics 181: 1378–1386
22. Chen XJ, Chan SH, Khor KA (2004) Electrochim Acta 49:1851–1861
23. Kuharuangrong S, Dechakupt T, Aungkavattana P (2004) Mater Lett 58:1964–1970
24. Chen KF, Ai N, Jiang SP (2014) Int J Hydrog Energy 39:10349–10358
25. Tai LW, Nasrallah MM, Anderson HU, Sparlin DM, Sehlin SR (1995) Solid State Ionics 76:273–283
26. Leng YJ, Chan SH, Liu QL (2008) Int J Hydrog Energy 33:3808–3817
27. Zhao EQ, Jia Z, Zhao L, Xiong YP, Sun CW, Brito EM (2012) J Power Sources 219:133–139
28. Zhao EQ, Ma C, Yang W, Xiong YP, Li JQ, Sun CW (2013) Int J Hydrog Energy 38:6821–6829
29. Chiba R, Yoshimura F, Sakurai Y (1999) Solid State Ionics 124: 281–288
30. Huang B, Zhu XJ, Nie HW, Niu YR, Li Y, Cheng N (2013) J Power Sources 235:20–28
31. Huang D, Xu Q, Zhang F, Chen W, Liu HX, Zhou J (2006) Mater Lett 60:1892–1895
32. Boehm E, Bassat JM, Steil MC, Dordor P, Mauvy F, Grenier JC (2003) Solid State Sci 5:973–981
33. Zhao K, Wang YP, Chen M, Xu Q, Kim BH, Huang DP (2014) Int J Hydrog Energy 39:7120–7130
34. Nicollet C, Flura A, Vibhu V, Rougier A, Bassat JM, Grenier JC (2015) J Power Sources 294:473–482
35. Kaluzhskikh MS, Kazakov SM, Mazo GN, Istomin SY, Antipov EV, Gippius AA (2011) J Solid State Chem 184:698–704
36. Sun C, Li Q, Sun LP, Zhao H, Huo LH (2014) Mater Res Bull 53: 65–69
37. Kolchina LM, Lyskov NV, Petukhov DI, Mazo GN (2014) J Alloys Compd 605:89–95
38. Shi Z, Xia T, Meng FC, Wang JP, Lian J, Zhao H, Bassat JM, Grenier JC, Meng J (2014) Fuel Cells 14:979–990
39. Shi Z, Xia T, Meng FC, Wang JP, Wu SM, Lian J, Zhao H, Xu CB (2015) Electrochim Acta 174:608–614
40. Souza RA, Kilner JA (1998) Solid State Ionics 106:175–187
41. Souza RA, Kilner JA (1999) Solid State Ionics 126:153–161
42. Takeda Y, Kanno R, Noda M, Yamamoto O (1987) J Electrochem Soc 134:2656–2661
43. Kim JD, Kim GD, Moon JW, Park Y, Lee WH, Kobayashi K, Nagai M, Kim CE (2001) Solid State Ionics 143:379–389